Structural and Multidisciplinary Optimization (2019) 60:1059–1077
https://doi.org/10.1007/s00158-019-02256-0

RESEARCH PAPER

An online variable-fidelity optimization approach for multi-objective design optimization

Leshi Shu[1] · Ping Jiang[1] · Qi Zhou[2] · Tingli Xie[1]

Received: 30 October 2018 / Revised: 28 February 2019 / Accepted: 6 March 2019 / Published online: 9 May 2019

Abstract

Multi-objective genetic algorithms (MOGAs) are effective ways for obtaining Pareto solutions of multi-objective design optimization problems. However, the high computational cost of MOGAs limits their applications to practical engineering optimization problems involving computational expensive simulations. To address this issue, a novel variable-fidelity (VF) optimization approach for multi-objective design optimization is proposed, in which a VF metamodel is embedded in the computation process of MOGA to replace the expensive simulation model. The VF metamodel is updated in the optimization process of MOGA, considering the cost of simulation models with different fidelity and the influence of the VF metamodel uncertainty. A normalized distance constraint is introduced to avoid selecting clustered sample points. Four numerical examples and two engineering cases are used to demonstrate the applicability and efficiency of the proposed approach. The results show that the proposed approach can obtain Pareto solutions with good quality and outperforms the other four approaches considered here as references in terms of computational efficiency.

Keywords Multi-objective optimization · Variable-fidelity optimization · Multi-objective genetic algorithms · Metamodel uncertainty

Nomenclature

$\boldsymbol{C}(\boldsymbol{x})$	the difference between HF response and prediction value of LF metamodel at x
$\hat{\boldsymbol{C}}(\boldsymbol{x})$	the prediction value of the scaling function metamodel at x
F_{Motor}	the weight of the engine in the front of the micro-aerial vehicle (N)
F_{Payload}	the payload of the micro-aerial vehicle (N/mm^2)
F_{Tail}	the weight of the tail of the micro-aerial vehicle (N)
$\boldsymbol{f}_h$	vector of HF responses of given HF sample set
$\boldsymbol{f}_l$	vector of LF responses of given LF sample set
$f_h(\boldsymbol{x})$	the function value of HF model at x
$\hat{f}_l(\boldsymbol{x})$	the prediction value of LF metamodel at x
$\hat{f}_{vf}(\boldsymbol{x})$	the prediction value of VF metamodel at x
$I(x)$	the prediction interval of VF metamodel at x
P1, P2	forces placed at the center of the right end of the torque arm (N)
$\boldsymbol{x}_l$	LF sample set
$\boldsymbol{x}_h$	HF sample set
$\sigma_C(\boldsymbol{x})$	the standard deviation of scaling function metamodel at x
$\sigma_l(\boldsymbol{x})$	the standard deviation of LF metamodel at x
$\sigma_{vf}(\boldsymbol{x})$	the standard deviation of VF metamodel at x

Subscripts

h	quantities associated with high fidelity
l	quantities associated with low fidelity
vf	quantities associated with variable fidelity

Responsible Editor: Shapour Azarm

✉ Qi Zhou
qizhouhust@gmail.com

[1] The State Key Laboratory of Digital Manufacturing Equipment and Technology, School of Mechanical Science and Engineering, Huazhong University of Science & Technology, Wuhan 430074, People's Republic of China

[2] School of Aerospace Engineering, Huazhong University of Science & Technology, Wuhan 430074, Hubei, People's Republic of China

1 Introduction

In engineering design optimization, multiple design objectives may be conflicting. The ability to rapidly understand trade-offs between multiple conflicting objectives is emphasized (Liu and Collette 2014). Multi-objective genetic algorithms

(MOGAs) are commonly used to solve these problems to find a set of optimum solutions in Pareto sense, that is, there is no optimum that is more superior than the other designs in all objectives (Shan and Wang 2005). Some MOGAs, such as NSGA-II (Ak et al. 2013; Deb et al. 2002), have proved to be very robust in converging to the true Pareto optimal sets. The main disadvantage of MOGAs is that they require a large amount of computational cost, especially when applied to design problems with time-consuming simulation models (Cheng et al. 2015a; Sun et al. 2013). A common used strategy to improve the efficiency of MOGAs is using metamodels (An et al. 2018), e.g., Kriging model (Li et al. 2009; Li 2011; Sun et al. 2017), radial basis function (RBF) (Chen et al. 2012; Datta and Regis 2016; Regis 2014), artificial neural networks (Song et al. 2012), support vector regression (SVR) (Andrés et al. 2012), and polynomial-based approximations (Goel et al. 2007; Rahmani et al. 2018), to replace the simulation models.

To replace original fitness functions, the metamodels must be accurate and efficient. Many researchers suggested the use of an online metamodel for fitness approximation (Li et al. 2008; Shi and Reitz 2010; Wang et al. 2016; Zhu et al. 2013). The online type constructs an initial metamodel firstly and then adaptively updates the metamodel during the optimization process (Hamdaoui et al. 2015; Li et al. 2009). Various model-updating strategies in metamodel-assisted MOGAs have been developed. Li et al. (2007) proposed a Kriging metamodel-assisted MOGA (K-MOGA), in which the individuals whose domination status may change are sent for high-fidelity simulations. Furthermore, Li (2011) proposed an improved kriging-assisted MOGA, in which a criterion is proposed to determine whether to use metamodel or simulation to calculate fitness values based on a measure of metamodel uncertainty. Luo et al. (2018) proposed an evolutionary optimization approach based on a multi-task Gaussian process regression model, which infers multiple subproblems jointly. Sun et al. (2017) proposed a RBF-assisted cooperative swarm optimization algorithm, in which surrogate-assisted and social learning-based particle swarm optimization algorithms share the evaluations by original fitness functions and focus on exploration and local search, respectively.

In metamodel-based design optimization, designers need to choose models with reasonable fidelities to obtain the response of the system. Generally, high-fidelity (HF) simulation models can provide more reliable and accurate simulation results than low-fidelity (LF) simulation models. However, HF models are more time-consuming than LF ones. Adopting a single-fidelity metamodel based on HF simulation sample points may be time-consuming, while relying on cheap LF simulation sample points may lead to unreliable optimal solutions (Shu et al. 2018). An alternative is using VF metamodel approaches to make a trade-off between high accuracy and efficiency (Gano et al. 2006; Han et al. 2010; Huang et al. 2006; Zhou et al. 2015). Liu and Collette (2014) proposed a metamodel management strategy to ensure the metamodel accuracy, in which k-means clustering algorithm is used to partition model data into local metamodels. Zhu et al. (2013) proposed a variable-fidelity optimization approach for MOGA (VFOS-MOGA), in which a metamodel is used to correct the LF models to the HF models. However, these VF metamodel-based multi-objective evolutional algorithms ignored the computational cost of LF sample points. Shu et al. (2018) proposed an online VF metamodel-assisted MOGA (OLVFM-MOGA) considering the possible change of domination status between dominated individuals and non-dominated individuals. However, this approach neglected the influence of the metamodel uncertainty on the domination status among the non-dominating individuals.

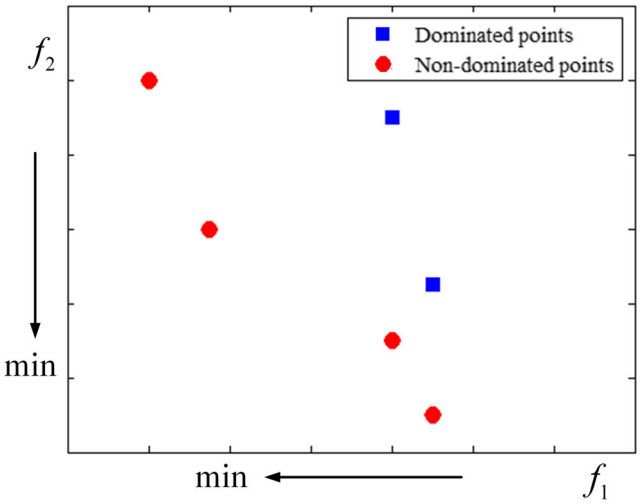

Fig. 1 Dominated individuals and non-dominated individuals

In this work, a novel VF optimization approach for multi-objective design optimization is proposed to ease the computational burden of MOGA. In the proposed approach, the NSGA-II is used as the original MOGA and a VF metamodel is embedded in the computation process of NSGA-II to evaluate fitness values. To improve the quality of optimization results, two novel model updating strategies, considering the VF metamodel uncertainty and the computational cost of HF/LF models, are proposed to update the VF metamodel in the optimization process. To avoid oversampling and improve efficiency, a constraint for new sample points is introduced. The performance of the proposed approach is tested, and the main advantages of the proposed approach are analyzed and summarized.

The rest of this paper is organized as follows. The next section presents the background and terminology. The subsequent section introduces the proposed approach. Then the proposed approach is tested using four numerical examples and two engineering examples, followed by concluding remarks in the last section.

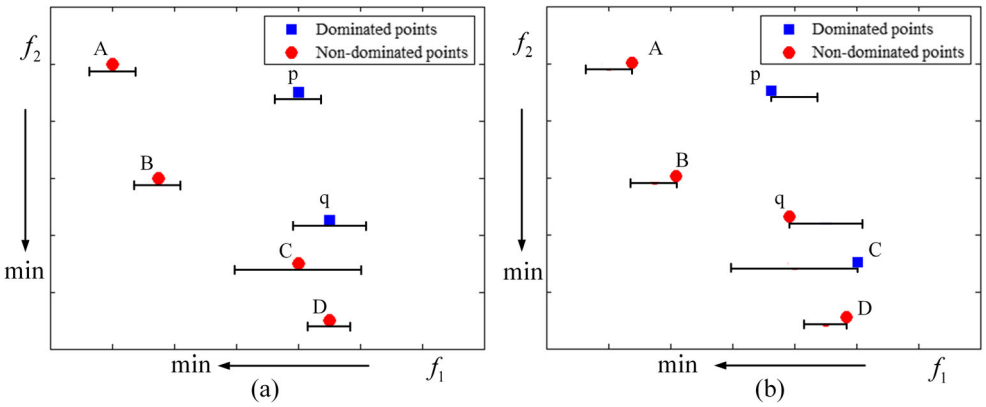

Fig. 2 **a** Prediction intervals of different individuals and **b** the possible changes of domination status of different individuals

2 The additive scaling function-based VF metamodel approach

A commonly used VF metamodel approach based on additive scaling function is used in this paper, in which the VF metamodel is obtained by tuning the LF metamodel using scaling function according to response values of the HF model. The VF metamodel can be expressed by,

$$\hat{\boldsymbol{f}}_{vf}(\boldsymbol{x}) = \hat{\boldsymbol{f}}_{l}(\boldsymbol{x}) + \hat{\boldsymbol{C}}(x) \tag{1}$$

where $\hat{\boldsymbol{f}}_{vf}(\boldsymbol{x})$ is the VF metamodel, $\hat{\boldsymbol{f}}_{l}(\boldsymbol{x})$ represents the LF metamodel, and $\hat{\boldsymbol{C}}(\boldsymbol{x})$ is the scaling function. Kriging models (Ollar et al. 2017) are used to construct the LF metamodel and scaling function metamodel in this paper.

Based on the LF sample points $x_l = \{\boldsymbol{x}_{l,1}, \boldsymbol{x}_{l,2}, \ldots, \boldsymbol{x}_{l,m_l}\}$ and their LF responses $\boldsymbol{f}_l = \{f_{l,1}, f_{l,2}, \ldots, f_{l,m_l}\}$, the LF metamodel $\hat{\boldsymbol{f}}_{l}(\boldsymbol{x})$ can be constructed. Based on the HF sample points $\boldsymbol{x}_h = \{\boldsymbol{x}_{h,1}, \boldsymbol{x}_{h,2}, \ldots, \boldsymbol{x}_{h,m_h}\}$ and their responses $\boldsymbol{f}_h = \{f_{h,1}, f_{h,2}, \ldots, f_{h,m_h}\}$, the discrepancies $\boldsymbol{C}(\boldsymbol{x}_h) = \{c(\boldsymbol{x}_{h,1}), c(x_{h,2}), \ldots, c(\boldsymbol{x}_{h,m_h})\}$ between the HF responses and LF predictions at the location $\boldsymbol{x}_{h,\,i}$ can be calculated by,

$$c(\boldsymbol{x}_{h,i}) = f_h(\boldsymbol{x}_{h,i}) - \hat{f}_l(\boldsymbol{x}_{h,i}) \tag{2}$$

Based on $\boldsymbol{x}_h$ and $\boldsymbol{C}(\boldsymbol{x}_h)$, the scaling function $\hat{C}(x)$ can be constructed using the Kriging model (Ollar et al. 2017). The Kriging model can provide an estimation of the prediction error on an unobserved point. The standard deviation of the prediction of the VF metamodel can be expressed by,

$$\sigma_{vf}(\boldsymbol{x}) = \sqrt{\sigma_l^2(\boldsymbol{x}) + \sigma_C^2(\boldsymbol{x})} \tag{3}$$

where $\sigma_l(\boldsymbol{x})$ and $\sigma_C(\boldsymbol{x})$ are the standard deviation of the LF metamodel and the scaling function metamodel, which can be predicted by Kriging models. The prediction interval of design point x can be defined as,

Table 1 The algorithm for selecting candidate HF/LF sample points in the exploration stage of MOGA

Algorithm 1		
Input: the individuals in the current generation.		
1	Begin	
2	$\{A, B, C \ldots\}_{non-dominated}$, $\{p, q, \ldots\}_{dominated}$	←Obtain the non-dominated individuals and dominated individuals by NSGA-II.
3	$I(A)$, $I(B)$, $I(C)$... , $I(p)$, $I(q)$, ...	←Calculate the prediction intervals of all individuals
4	$A, B, C \ldots, p, q, \ldots$	←Calculate the positions with best objective value of dominated individuals and the positions with worst objective value of non-dominated individuals
5	$\{A, B, q, \ldots\}_{non-dominated}$, $\{p, C, \ldots\}_{dominated}$	←Sort the population and obtain the non-dominated individuals and dominated individuals
6	$CP_l = \{C, q\}$	←The individuals whose domination status may change will be selected as candidate LF sample points
7	$I(C)$, $I(q)$	← Recalculate the prediction intervals
8	$A, B, C \ldots, p, q, \ldots$	←Recalculate the positions with best objective value of dominated individuals and the positions with worst objective value of non-dominated individuals
9	$\{A, B, C, q, \ldots\}_{non-dominated}$, $\{p, \ldots\}_{dominated}$	←Sort the population and obtain the non-dominated individuals and dominated individuals
10	$CP_h = \{\mathrm{q}\}$	←The individuals whose domination status may change will be selected as candidate HF sample points

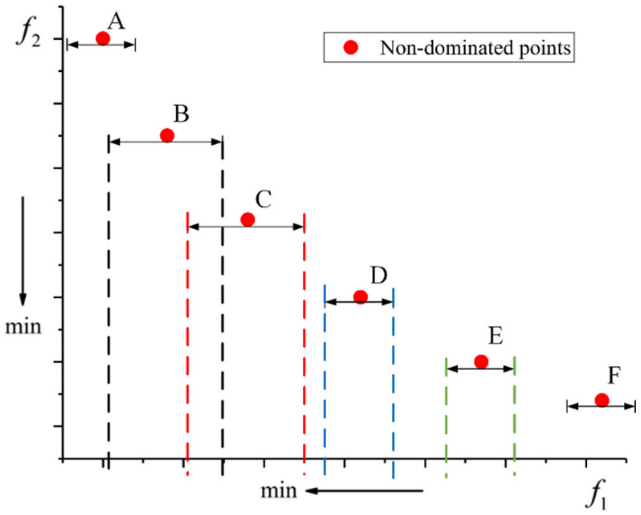

Fig. 3 Prediction intervals of non-dominated individuals

$$\begin{cases} I(\boldsymbol{x}) = c\sigma_{vf}(\boldsymbol{x}) \\ \boldsymbol{f}(\boldsymbol{x}) = \hat{\boldsymbol{f}}_{vf}(\boldsymbol{x}) \pm 0.5I(\boldsymbol{x}) \end{cases} \tag{4}$$

where c reflects the confidence level, $I(x)$ is the prediction interval. According to the six-sigma criterion in engineering design (Koch et al. 2004), the value of c is set to 6 in this paper and this represents a confidence level of 99.87% that the true response is within the prediction interval.

3 The proposed approach

In this section, the details of the proposed approach are presented. The optimization process of MOGA is divided into exploration stage and exploitation stage. For each stage, a strategy is proposed to select candidate HF/LF sample points (see section 3.1 and 3.2). Then, a constraint for the candidate sample points is introduced in section 3.3, followed by the steps of the proposed approach in section 3.4. The differences between the proposed approach and OLVFM-MOGA are analyzed in section 3.5.

3.1 Selecting candidate HF/LF sample points in exploration stage

In any generation of MOGA, fitness values of all individuals are evaluated by the simulation model or VF metamodel. Based on these predicted values, the dominance status can be determined as follows in Fig. 1.

At the beginning of the MOGA, there are many dominated solutions in the population. When the number of non-dominated individuals is less than r% of the total individuals, we define this stage as exploration stage. r is a predefined value and the selecting of r is introduced in section 4.3.

At this stage, the relationship between the dominated solutions and the non-dominated solutions, which is affected by

Table 2 The algorithm for selecting candidate HF/LF sample points in the exploitation stage of MOGA

Algorithm 2	
Input: the individuals in the current generation.	
1 Begin	
2 $\{..., \boldsymbol{x}_{i-1}, \boldsymbol{x}_i, \boldsymbol{x}_{i+1}, ...\}_{non-dominated}$	←Obtain the non-dominated individuals and sort them by f_1 (suppose f_1 is calculated by VF metamodel)
3 ..., $I(\boldsymbol{x}_{i-1})$, $I(\boldsymbol{x}_i)$, $I(\boldsymbol{x}_{i+1})$, ...	←Calculate the prediction intervals of non-dominated individuals
4 For $i = 1: n$	←n is the total number of non-dominated individuals
5 If $\begin{cases} \frac{1}{2}(I(\boldsymbol{x}_{i-1}) + I(\boldsymbol{x}_i)) <= \lvert \boldsymbol{f}_1(\boldsymbol{x}_{i-1}) - \boldsymbol{f}_1(\boldsymbol{x}_i) \rvert (if\ 2 < i < n) \\ \frac{1}{2}(I(\boldsymbol{x}_i) + I(\boldsymbol{x}_{i+1})) <= \lvert \boldsymbol{f}_1(\boldsymbol{x}_i) - \boldsymbol{f}_1(\boldsymbol{x}_{i+1}) \rvert (if\ 1 < i < n-1) \end{cases}$	←Judge whether the domination status of an individual may change.
6 $\boldsymbol{CP}_l = \{\boldsymbol{CP}_l, \boldsymbol{x}_i\}$	←The individuals whose domination status may change will be selected as candidate LF sample points.
7 End for	
8 ..., $I(\boldsymbol{x}_{i-1})$, $I(\boldsymbol{x}_i)$, $I(\boldsymbol{x}_{i+1})$, ...	←Recalculate the prediction intervals of these individuals
9 For $i = 1: n$	
10 If $\begin{cases} \frac{1}{2}(I(\boldsymbol{x}_{i-1}) + I(\boldsymbol{x}_i)) <= \lvert \boldsymbol{f}_1(\boldsymbol{x}_{i-1}) - \boldsymbol{f}_1(\boldsymbol{x}_i) \rvert (if\ 2 < i < n) \\ \frac{1}{2}(I(\boldsymbol{x}_i) + I(\boldsymbol{x}_{i+1})) <= \lvert \boldsymbol{f}_1(\boldsymbol{x}_i) - \boldsymbol{f}_1(\boldsymbol{x}_{i+1}) \rvert (if\ 1 < i < n-1) \end{cases}$	←Judge whether the domination status of an individual may change.
11 $\boldsymbol{CP}_h = \{\boldsymbol{CP}_h, \ \boldsymbol{x}_i\}$	←The individuals whose domination status may change will be selected as candidate HF sample points.
12 **End for**	

Table 3 The algorithm for selecting HF/LF sample points which meet the distance constraint

Algorithm 3

Input: the HF/LF points newly selected by algorithm 1 and algorithm 2; the existing HF/LF points

1	Begin	
2	Candidate LF sample points $\boldsymbol{CP}_l = \{CP_{l,1}\ CP_{l,2}\ \ldots\ CP_{l,nl}\}$ Candidate HF sample points $\boldsymbol{CP}_h = \{CP_{h,1}\ CP_{h,2}\ \ldots\ CP_{h,nh}\}$ Existing LF points $\boldsymbol{LP} = \{LP_1\ LP_2\ \ldots\ LP_{ml}\}$ Existing HF points $\boldsymbol{HP} = \{HP_1\ HP_2\ \ldots\ HP_{mh}\}$	← Candidate HF/LF sample points are sorted in descending order of prediction intervals.
3	For $i = 1{:}nl$	
4	min_dis($CP_{l,i}$,LP)	←Calculate the minimum distance between $CP_{l,i}$ and existing LF points
5	If min_dis($CP_{l,i}$,LP) > δ	
6	$LP = \{LP\ CP_{l,i}\}$	←$CP_{l,i}$ will be sent for LF simulation.
7	End if	
8	End for	
9	For $i = 1{:}nh$	
10	min_dis($CP_{h,i}$,HP)	←Calculate the minimum distance between $CP_{h,i}$ and existing HF points
11	If min_dis($CP_{h,i}$,HP) > δ	
12	$HP = \{HP\ CP_{h,i}\}$	←$CP_{h,i}$ will be sent for HF simulation.
13	**End if**	
14	**End for**	

the metamodel prediction interval, is very important to ensure the correct evolutionary direction. Suppose that f_1 is calculated by the VF metamodel, the prediction intervals of individuals are shown in Fig. 2 a. To show the possible change of the domination status, the dominated individuals are moved to possible locations with best objective values while the non-dominated individuals are moved to possible locations with worst objective values as shown in Fig. 2 b. It should be noted that if the two objectives are replaced by VF metamodels, the prediction interval of an individual will become a rectangle. Then, we can still find the possible position with the best or worst objective values. Similarly, if there are more than two objectives replaced by the VF metamodel, the prediction interval of an individual will become a cuboid or hyper-cuboid.

It can be seen in Fig. 2 b that domination status of some individuals may change while that of others may not. The

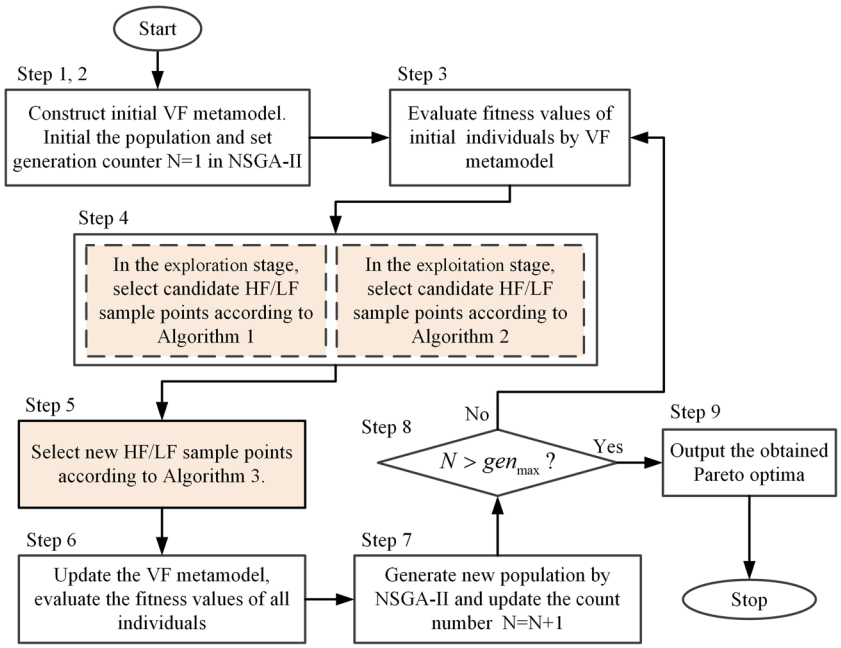

Fig. 4 Flowchart of the proposed approach

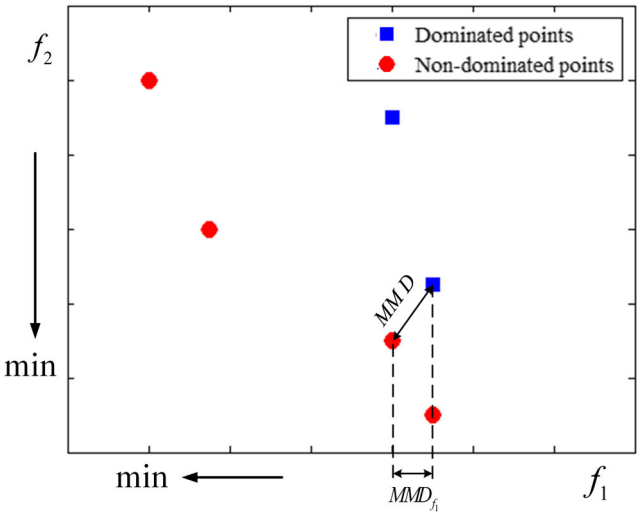

Fig. 5 Projected MMD in OLVFM-MOGA

prediction intervals of individuals whose domination status may change (see points C and q) should be reduced. According to (3) and (4), the prediction intervals can be reduced by sending the individuals for LF or HF simulations. Considering that the computational cost of the LF model is much less than that of the HF model, the individuals whose domination status may change will be selected as candidate LF sample points first. To estimate the prediction interval after LF simulations, the prediction responses at the candidate LF sample points are treated as if they were the true responses in updating the VF metamodel (Zhou et al. 2017). Thus, the prediction interval of the VF metamodel can be estimated by (5),

$$\begin{cases} \sigma_{vf}(\boldsymbol{x}) = \sigma_c(\boldsymbol{x}) \\ I(\boldsymbol{x}) = c\sigma_{vf}(\boldsymbol{x}) \\ \boldsymbol{f}(\boldsymbol{x}) = \hat{\boldsymbol{f}}_{vf}(\boldsymbol{x}) \pm 0.5I(\boldsymbol{x}) \end{cases} \tag{5}$$

According to the prediction interval $I(x)$ in (5), the same way can be used to judge whether an individual's domination status may change. If the domination status of the individual may change, the prediction interval should be further reduced and the individual will be selected as candidate HF sample points. The algorithm of selecting such individuals for candidate HF/LF sample points is listed in Table 1.

Output: candidate LF sample points CP_l and HF sample points CP_h

3.2 Selecting candidate HF/LF sample points in exploitation stage

As MOGA proceeds, the number of non-dominated individuals is increasing and the Pareto solutions approach converges. When the number of non-dominated individuals is more than r% of the total individuals, we define this stage as exploitation stage. It is necessary to focus on the influence of uncertainty on the relationship among non-dominated individuals to ensure the accuracy of the optimum solutions. Consider the relationship between an individual and its neighboring individuals, as illustrated in Fig. 3.

As shown in Fig. 3, the prediction intervals of non-dominated individuals are projected to the dimension in which the objective is replaced by the VF metamodel. It can be seen that the domination status of a point may change if its prediction interval coincides with the prediction intervals of the adjacent individuals (such as point B). If the domination status of a point x_i may not change (such as point D), the following conditions should be satisfied,

$$\begin{cases} \frac{1}{2}(\mathrm{I}(\boldsymbol{x}_{i-1}) + \mathrm{I}(\boldsymbol{x}_i)) <= \left| \boldsymbol{f}_1(\boldsymbol{x}_{i-1}) - \boldsymbol{f}_1(\boldsymbol{x}_i) \right| \ (if\, 2 < i < n) \\ \frac{1}{2}(\mathrm{I}(\boldsymbol{x}_i) + \mathrm{I}(\boldsymbol{x}_{i+1})) <= \left| \boldsymbol{f}_1(\boldsymbol{x}_i) - \boldsymbol{f}_1(\boldsymbol{x}_{i+1}) \right| \ (if\, 1 < i < n-1) \end{cases} \tag{6}$$

where x_{i-1} and x_{i+1} are two individuals adjacent to x_i. Similarly, the individuals whose domination status may change will be selected as candidate LF sample points first, and the prediction interval of the VF metamodel can be estimated by (5). The prediction interval of individuals will be reduced after LF simulations and then (6) will still be used to judge whether domination status of an individual may change. If the domination status of the individuals may still change, the individuals will be selected as candidate HF sample points. The algorithm of selecting such candidates for HF/LF sample points is listed in Table 2. NSGA-II is used to obtain the non-dominated individuals in the proposed approach. In Algorithm 2, if there are more than one objective that are replaced by VF metamodels, the non-dominated points can be sorted by any objective. Then, we can consider the influence of the prediction intervals in the direction of each objective.

Output: candidate LF sample points CP_l and HF sample points CP_h

It should be noted that there may be oscillations between the two stages in several generations. Since the proposed approach is not very sensitive to the value of r as demonstrated in 4.2.1 and MOGA usually requires many generations to converge to the Pareto solutions, this has little impact on the optimization results.

Table 4 The initial sample size for all examples

Parameter	NSGA-II with HF model	K-MOGA	VFOS-MOGA	OLVFM-MOGA	Proposed approach
Initial LF samples	–	–	–	60	60
Initial HF samples	–	40	–	20	20

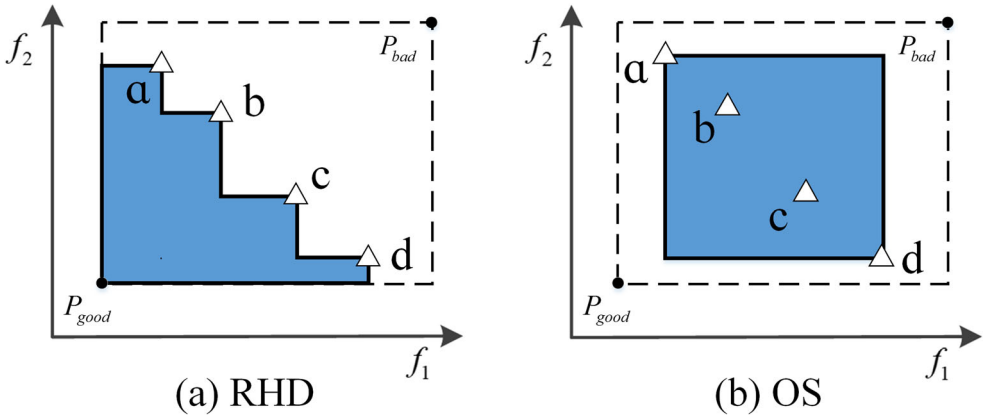

Fig. 6 Quality metrics **a** RHD and **b** OS

3.3 Constraint condition of newly selected sample points

Kriging models are used to construct the LF model and scaling function in this work. Two algorithms are proposed in section 3.1 and section 3.2 to select HF/LF sample points. It may cause the reduction of VF metamodel accuracy or unnecessary computational cost; the main reasons are as follows: (1) the sample points selected by the two algorithms may be very close in the design space. The cluster of sample points may cause oversampling for the Kriging model (Shu et al. 2017; Zhu et al. 2013). (2) When a sample point is used to update the Kriging model, the prediction error of unobserved points near this point will be reduced, that means, the points which are very close to other existing sample points should not be used to update the VF metamodel at the same time.

To prevent the cluster of sample points and improve efficiency, the points selected by the two algorithms are required to fall a certain distance away from the existing points. In this work, a Euclidean distance measure in independent variable space is used, which is normalized by the range between the upper and lower bounds. A normalized distance greater than δ from any existing sample points is required before a newly selected point is used to update the VF metamodel. In general, the higher the dimension of the problem is, the smaller the value of δ should be set. However, how to select a threshold value is subjective. We referred to some references (Shu et al. 2017; Zhu et al. 2013) and set δ=0.02n, where n is the number of the design variables. For the test problems, this setting can not only avoid unnecessary calculation cost, but also guarantee the accuracy of optimization solutions.

The algorithm of selecting HF/LF sample points that meet the requirements is listed in Table 3.

Output: individuals which will be sent for LF analysis (*LP*) and HF analysis (*HP*)

3.4 Steps of the proposed approaches

The flowchart of the proposed approach is demonstrated in Fig. 4. Optimal Latin hypercube design (OLHD) (McKay et al. 2000) is used to generate initial HF/LF sample points. The detailed steps are described as follows.

Begin

Step 1: Generate initial LF/HF sample points and obtain their responses to construct the initial VF metamodel.

Step 2: Initialize the population by NSGA-II. Set the generation count number $N = 1$.

Step 3: Evaluate fitness values of individuals by the constructed VF metamodel.

Step 4: When the number of non-dominated individuals is less than r% of the population size, select candidate HF/LF sample points according to Algorithm 1; when the number of non-dominated individuals is more than r% of the

Table 5 The settings of extreme good and bad points for all examples

Examples	P_{good}	P_{bad}
ZDT1/ZDT2/FON	(−0.2, −0.2)	(1.2, 1.2)
POL	(−2, −2)	(18, 28)
Design optimization of a torque arm	(350, 0.25)	(750, 2.4)
Design optimization of a micro-aerial vehicle fuselage	(165, 3.0)	(230, 7.0)

Table 6 Formulations of four numerical examples

Cases	Formulation
ZDT1	*minimize* $f_1(x) = x_1$ $\mathrm{HF}: f_2(x) = g(x) \times h(x)$ $\mathrm{LF}: f_2(x) = (0.8g(x) - 0.2) \times (1.2h(x) + 0.2)$ *where* $g(x) = 1 + \frac{9}{n-1}\sum_{i=2}^{n} x_i$ $h(x) = 1 - \sqrt{f_1(x)/g(x)}$ $n = 3$ $0 \le x_i \le 1, i = 1\ldots, n$
ZDT2	*minimize* $f_1(x) = x_1$ $\mathrm{HF}: f_2(x) = g(x) \times h(x)$ $\mathrm{LF}: f_2(x) = \left(0.9^{*} g(x) + 1.1\right) \times \left(1.1^{*} h(x) - 0.1\right)$ *where* $g(x) = 1 + \frac{9}{n-1}\sum_{i=2}^{n} x_i$ $h(x) = 1 - \sqrt{f_1(x)/g(x)}$ $n = 3$ $0 \le x_i \le 1, i = 1\ldots, n$
FON	*minimize* $f_1(x) = 1 - \exp\left(-\sum_{i=1}^{3}\left(x_i - \frac{1}{\sqrt{3}}\right)^2\right)$ $\mathrm{HF}: f_2(x) = 1 - \exp\left(-\sum_{i=1}^{3}\left(x_i + \frac{1}{\sqrt{3}}\right)^2\right)$ $\mathrm{LF}: f_2(x) = (1 - \exp(-(x_1 + 0.5)^2 - (x_2 + 0.55)^2 - (x_3 + 0.6)^2)) \cdot (1.1 + 0.25\sin x_1)$ $-4 \le x_i \le 4, i = 1, \ldots, 3$ *where* $g(x) = 1 + \frac{9}{n-1}\sum_{i=2}^{n} x_i$ $h(x) = 1 - \sqrt{f_1(x)/g(x)}$ $n = 3$ $0 \le x_i \le 1, i = 1\ldots, n$
POL	*minimize* $\mathrm{HF}: f_1(x) = \left[1 + (A_1 - B_1)^2 + (A_2 - B_2)^2\right]$ $\mathrm{LF}: f_1(x) = \left[1 + (0.9A_1 - 1.2B_1)^2 + 0.9(1.2A_2 - 0.9B_2)^2\right]$ $f_2 = (x) = (x_1 + 3)^2 + (x_2 + 1)^2$ *where* $A_1 = 0.5\sin 1 - 2\cos 1 + \sin 2 - 1.5\cos 2$ $A_2 = 1.5\sin 1 - \cos 1 + 2\sin 2 - 0.5\cos 2$ $B_1 = 0.5\sin x_1 - 2\cos x_1 + \sin x_2 - 1.5\cos x_2$ $B_2 = 1.5\sin x_1 - \cos x_1 + 2\sin x_2 - 0.5\cos x_2$ $-\pi \le x_i \le \pi, i = 1, 2$

population size, select candidate HF/LF sample points according to Algorithm 2.

Step 5: Select new HF/LF sample points according to Algorithm 3.

Step 6: Update the VF metamodel, evaluate the fitness values of all individuals by the VF metamodel.

Step 7: Generate the next generation of population by NSGA-II, update $N = N + 1$.

Step 8: Check whether the stopping criterion is satisfied: If yes, go to Step 9; otherwise, go back to Step 3.

Step 9: Output the obtained Pareto optima.

End

3.5 Differences between the proposed approach and OLVFM-MOGA

The proposed approach is an improved version of the author's previous work, the OLVFM-MOGA (Shu et al. 2018). In

Table 7 Quality metrics of optimization results of proposed approach under different value of r

Cases	Metrics	Proposed approach (r% = 60%)			Proposed approach (r% = 70%)			Proposed approach (r% = 80%)			Proposed approach (r% = 90%)		
		30 runs	Mean	STD	30 runs	Mean	STD	30 runs	Mean	STD	30 runs	Mean	STD
ZDT1	RHD	(0.25 0.37)	0.34	0.04	(0.25 0.39)	0.34	0.03	(0.30 0.37)	0.35	0.02	(0.28 0.38)	0.34	0.02
	OS	(0.12 0.51)	0.38	0.12	(0.15 0.59)	0.40	0.11	(0.20 0.53)	0.43	0.09	(0.20 0.52)	0.39	0.09
	FC	(52.75 105.75)	77.96	14.84	(55 116)	77.56	15.79	(54 111.5)	77.23	12.19	(58.75 93.75)	78.09	8.73
ZDT2	RHD	(0.35 0.56)	0.52	0.05	(0.50 0.54)	0.53	0.01	(0.53 0.55)	0.54	0.00	(0.44 0.55)	0.53	0.02
	OS	(0.04 0.61)	0.45	0.15	(0.53 0.55)	0.48	0.07	(0.34 0.54)	0.50	0.03	(0.12 0.59)	0.47	0.10
	FC	(46.5 85.25)	65.23	10.20	(47 92.5)	67.41	13.12	(46.75 82.75)	68.02	9.07	(48 94)	68.73	12.61
FON	RHD	(0.43 0.64)	0.51	0.04	(0.37 0.61)	0.52	0.05	(0.46 0.57)	0.53	0.02	(0.45 0.63)	0.52	0.03
	OS	(0.18 0.59)	0.36	0.11	(0.23 0.61)	0.40	0.10	(0.29 0.60)	0.40	0.07	(0.25 0.62)	0.39	0.08
	FC	(45.75 66.75)	54.47	5.00	(46.5 65)	54.91	4.47	(44.25 69)	55.14	6.24	(42.25 65.25)	54.35	4.91
POL	RHD	(0.09 0.25)	0.23	0.03	(0.23 0.25)	0.23	0.00	(0.23 0.25)	0.23	0.00	(0.23 0.25)	0.23	0.00
	OS	(0.08 0.75)	0.65	0.11	(0.64 0.75)	0.66	0.02	(0.65 0.74)	0.66	0.02	(0.65 0.74)	0.66	0.02
	FC	(64.75106)	81.53	9.78	(67.5 103.5)	82.57	9.49	(62.25 107.75)	83.68	12.72	(66.50 99.25)	82.84	8.38

OLVFM-MOGA, the minimum of minimum distance (MMD), which refers to the minimum distance of all distances between all pairs of non-dominated points and dominated points, is calculated first for the current non-dominated and dominated points. Then, the MMD is projected to a dimension in which the objective is replaced by the VF metamodel as shown in Fig. 5.

The current individuals are sorted in descending order according to the prediction intervals expressed as,

$$I_p(x_1) \geq I_p(x_2) \geq \ldots \geq I_p(x_{n-1}) \geq I_p(x_n) \tag{7}$$

In OLVFM-MOGA, if $I_p(x_n) + I_p(x_{n-1}) > MMD_{f_1}$, x_n will be considered as the point whose domination status is uncertain and be sent for the LF or HF simulation. According to the criterion, point A, B, C, p, and q will be selected for simulations. However, as shown in Fig. 2, the domination status of point A, B, and q may not change due to the prediction intervals; this indicates that the OLVFM-MOGA may cause a waste of computational cost for selecting points with uncertain domination status. For this shortcoming, a VF metamodel updating strategy is developed in the proposed approach which can judge whether the dominant state of the individuals may change more rationally as presented in section 3.1.

When there are no dominated points in the current population, no matter how large the prediction intervals of the individuals, they will not be sent for simulations in OLVFM-MOGA. This may lead to unreliable Pareto solutions. For this shortcoming, a VF metamodel updating strategy focusing on the influence of prediction intervals on the relationship among non-dominated individuals is presented in section 3.2 to ensure the accuracy of Pareto solutions.

In OLVFM-MOGA, the individuals sent for simulations may be very close in the design space. When a point is used to update the VF metamodel, the prediction error of unobserved points near this point will be reduced. This means that sending individuals that are very close in the design space for simulation simultaneously is unnecessary. To save on computational cost, a constraint of the new selected sample points is introduced in section 3.3.

4 Examples and results

In this section, four numerical examples (ZDT1, ZDT2, FON, and POL problem) (Li 2011; Shu et al. 2018), an engineering

Table 8 Quality metrics of optimization results of NSGA-II with HF models for numerical examples

Cases	Metrics	NSGA-II with HF model		
		30 runs	Mean	STD
ZDT1	RHD	(0.34 0.39)	0.38	0.01
	OS	(0.35 0.51)	0.50	0.03
	FC	(3823 3864)	3840.93	10.46
ZDT2	RHD	(0.51 0.57)	0.55	0.01
	OS	(0.32 0.55)	0.5	0.04
	FC	(3785 3862)	3823.00	23.72
FON	RHD	(0.54 0.59)	0.56	0.01
	OS	(0.31 0.49)	0.46	0.04
	FC	(3819 3876)	3844.93	11.96
POL	RHD	(0.22 0.24)	0.23	0.01
	OS	(0.61 0.71)	0.63	0.04
	FC	(3813 3870)	3841.33	14.54

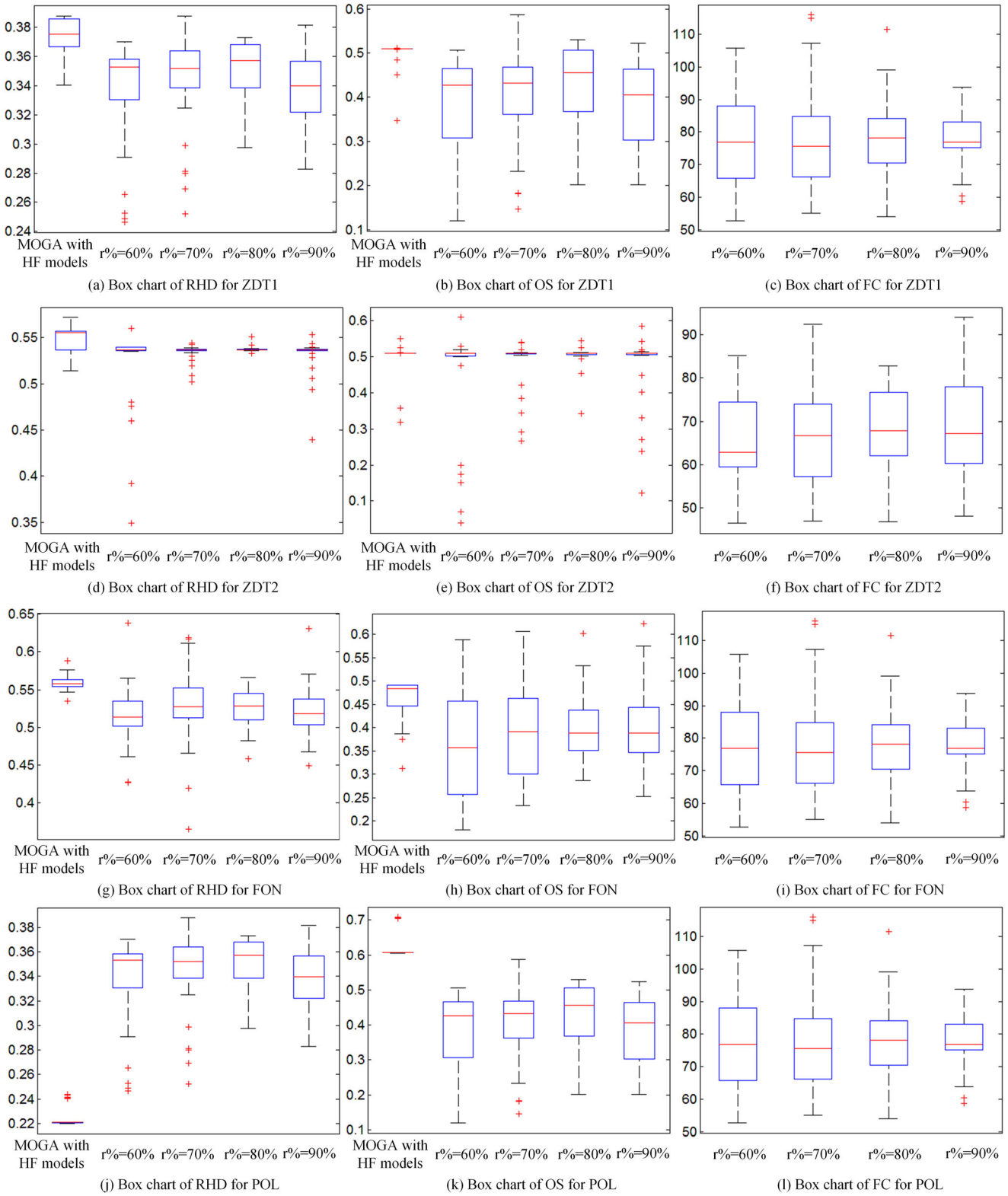

Fig. 7 Box charts of RHD, OS, and FC numerical examples under different value of r

case (design optimization of a torque arm) adapted from Park et al. (Park and Dang 2010), and another engineering case (design optimization of a micro-aerial vehicle fuselage) adapted from Nguyen et al. (2013) are used to demonstrate the applicability and efficiency of the proposed approach. For comparison, these examples are solved using other

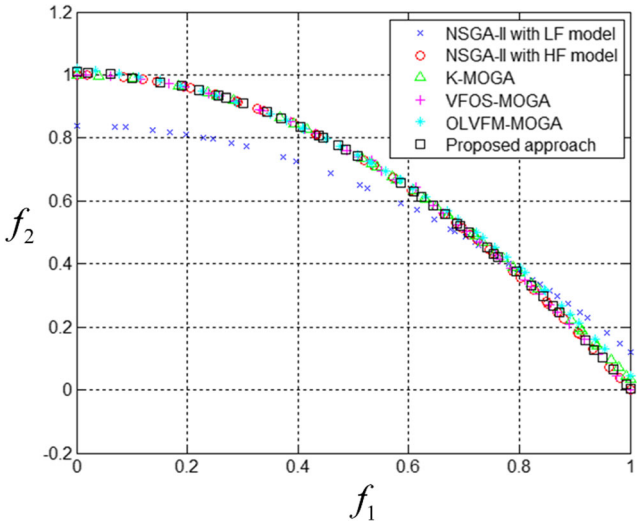

Fig. 8 The obtained Pareto frontiers of ZDT2 using different approaches

approaches: (1) NSGA-II with HF model, (2) K-MOGA, (3) VFOS-MOGA (Zhu et al. 2013), and (4) OLVFM-MOGA (Shu et al. 2018). The population size is set as 40 and the maximum generations is set as 100 for all the approaches. The settings for the initial sample size of different approaches are summarized in Table 4.

4.1 Quality and efficiency metrics

To compare the ability of obtaining Pareto frontiers and the efficiency of different approaches, three metrics, relative hyperarea difference (RHD), overall spread (OS), and function calls (FC), are calculated.

RHD and OS are used to measure the quality of Pareto frontiers (Cheng et al. 2015b; Wu and Azarm 2001). As shown in Fig. 6, RHD and OS represent the convergence and diversity of the obtained Pareto frontier, respectively. The smaller the value of RHD is, the higher convergence of the Pareto frontier is. The larger the value of OS is, the higher diversity of the Pareto frontier is. $P = \{a, b, c, d\}$ is the current Pareto set, and $p_{good}\, p_{bad}$ are the extreme good and bad points, respectively. The value of RHD and OS are calculated as follows,

$$RHD = \frac{HA\left(p_{\text{bad}}, p_{\text{good}}\right) - HA(p_{\text{bad}}, a, b, c, d)}{HA\left(p_{\text{bad}}, p_{\text{good}}\right)} \tag{8}$$

$$OS = \frac{HA[\text{extremes}(P)]}{HA\left(p_{\text{bad}}, p_{\text{good}}\right)} \tag{9}$$

where HA [extremes(P)] represents the area bounded by the two extreme points in Pareto frontier and $HA(p_{\text{bad}}, p_{\text{good}})$ represents the area bounded by p_{good} and p_{bad}.

The set of P_{good} and $P_{bad}$for all the examples is shown in Table 5.

FC denotes the number of simulation calls, and this indicates the computation cost of different approaches. Since some approaches adopt simulation models with different fidelity, the FC is calculated by (10):

Table 9 Comparison results of different approaches for ZDT2 problem

Metrics	K-MOGA			VFOS-MOGA			OLVFM-MOGA			Proposed approach		
	30 runs	Mean	STD	30 runs	Mean	STD	30 runs	Mean	STD	30 runs	Mean	STD
RHD	(0.50 0.57)	0.54	0.02	(0.48 0.59)	0.55	0.02	(0.53 0.56)	0.55	0.01	(0.53 0.54)	0.54	0.002
OS	(0.26 0.68)	0.51	0.06	(0.19 0.56)	0.48	0.09	(0.41 0.54)	0.50	0.02	(0.34 0.56)	0.51	0.03
FC	(98 210)	133.10	24.24	(1262.5 1292)	1277.03	6.81	(51.75 165.5)	104.70	24.83	(56 94.25)	80.83	8.61

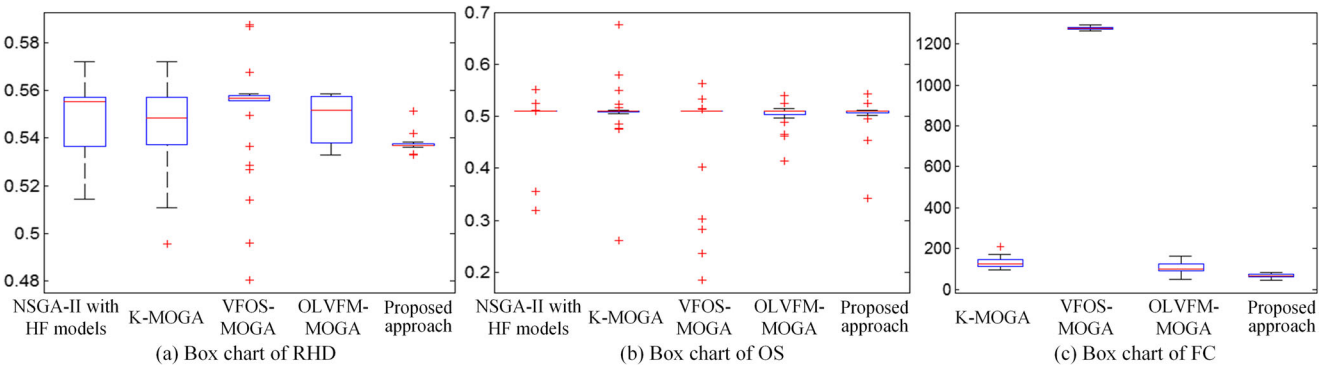

Fig. 9 The box charts of different approaches for ZDT2 problem

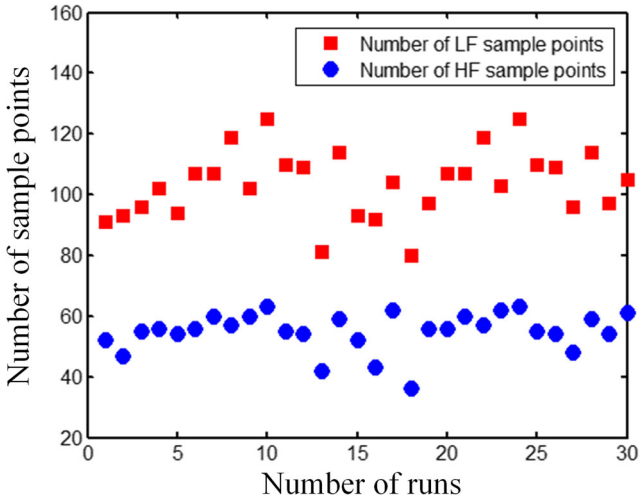

Fig. 10 The number of HF/LF sample points in the 30 runs of the proposed approach for ZDT2

$$FC = \frac{N_{LF}}{T} + N_{HF} \tag{10}$$

where N_{LF} is the number of LF simulation model calls and N_{HF} is the number of HF simulation model calls. Tdenotes the ratio between the computational cost of running HF simulation model and that of running LF simulation model.

4.2 Numerical examples

In the numerical examples, the LF model is a modified version of the real function and the computational cost of a HF sample is assumed to be four times of that of a LF sample (T=4). For the numerical example, $f_2(x)$ will be replaced by the VF metamodel in the metamodel-based optimization process. The formulations of four numerical examples are listed in Table 6.

4.2.1 Selecting the value of *r*

To demonstrate the influence of the value of r, we tested the effect of four different values (r% = 60%, 70%, 80%, 90%) on the optimization results. For each value of r, the optimization problems are solved 30 times and the quality metrics are listed in Table 7. To compare the quality of optimization results under different values of r, the NSGA-II with HF models is run 30 times and the optimization results can be seen as

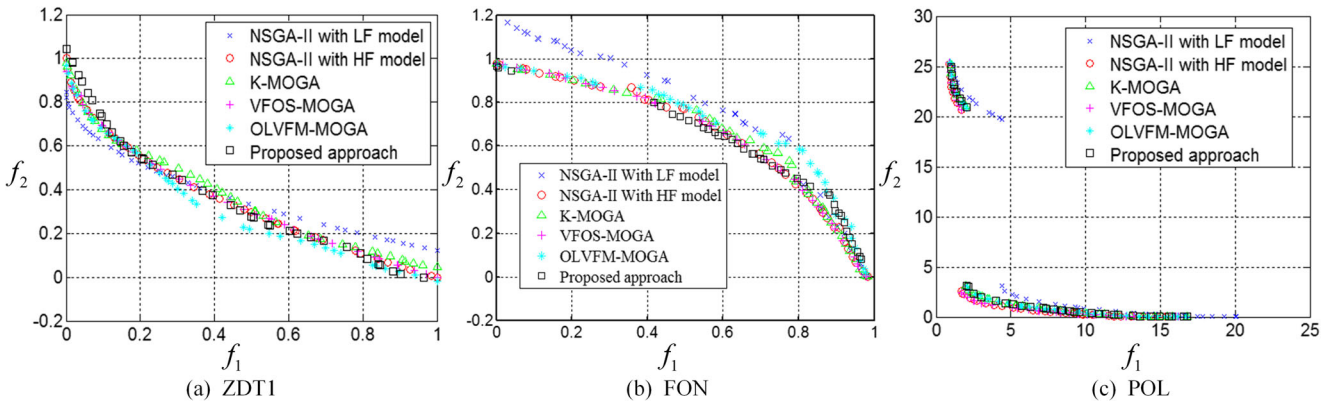

Fig. 11 The obtained Pareto frontiers of ZDT1, FON, and POL using different approaches

Table 10 Quality and efficiency metrics of different approaches for ZDT1, FON, and POL problems

		K-MOGA			VFOS-MOGA			OLVFM-MOGA			Proposed approach		
		30 runs	Mean	STD	30 runs	Mean	STD	30 runs	Mean	STD	30 runs	Mean	STD
ZDT1	RHD	(0.32 0.45)	0.37	0.03	(0.34 0.41)	0.39	0.01	(0.35 0.40)	0.37	0.02	(0.30 0.37)	0.35	0.02
	OS	(0.22 0.67)	0.44	0.11	(0.32 0.59)	0.51	0.05	(0.29 0.57)	0.46	0.07	(0.20 0.53)	0.43	0.09
	FC	(191 476)	323.63	81.55	(1284.5 1336.5)	1304.17	12.61	(137 439.5)	257.96	58.55	(54 111.5)	77.23	12.19
FON	RHD	(0.51 0.58)	0.56	0.01	(0.53 0.56)	0.55	0.01	(0.54 0.58)	0.56	0.01	(0.46 0.57)	0.53	0.02
	OS	(0.15 0.49)	0.42	0.10	(0.28 0.49)	0.46	0.06	(0.29 0.49)	0.42	0.07	(0.29 0.60)	0.40	0.07
	FC	(137 348)	249.20	54.48	(1331 1362.8)	1347.77	7.27	(83.75292)	169.91	55.48	(44.25 69)	55.14	6.24
POL	RHD	(0.23 0.26)	0.24	0.01	(0.23 0.27)	0.25	0.01	(0.23 0.26)	0.24	0.01	(0.23 0.25)	0.23	0.01
	OS	(0.65 0.74)	0.67	0.03	(0.58 0.75)	0.64	0.04	(0.61 0.74)	0.67	0.04	(0.65 0.74)	0.66	0.02
	FC	(78 142)	101.3	17.03	(1273.25 1292.5)	1283.36	3.98	(83.75 130.25)	104.9	11.61	(62.25 107.75)	83.68	12.72

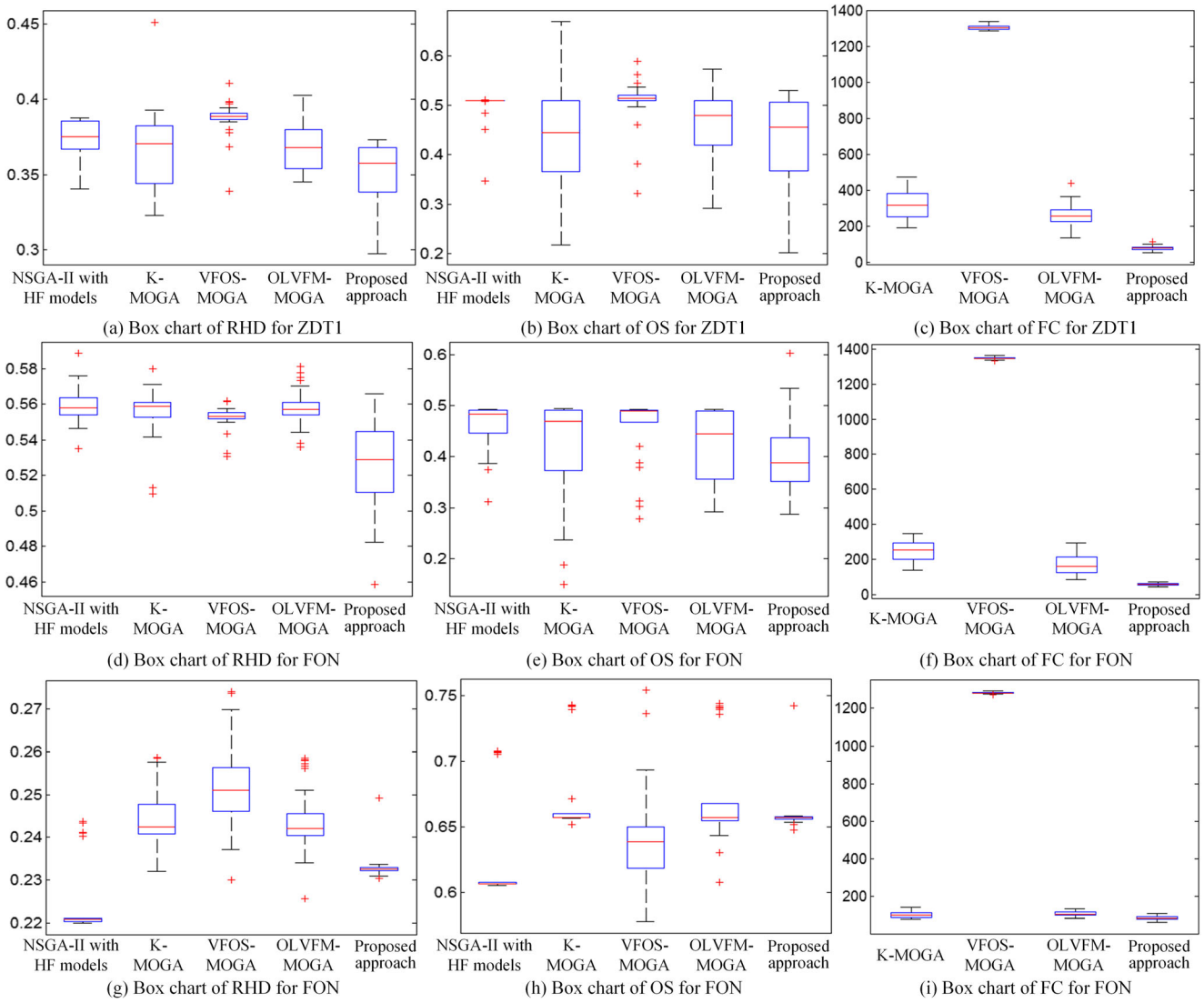

Fig. 12 Box charts of RHD, OS, and FC obtained by different approaches for ZDT1, FON, and POL problems

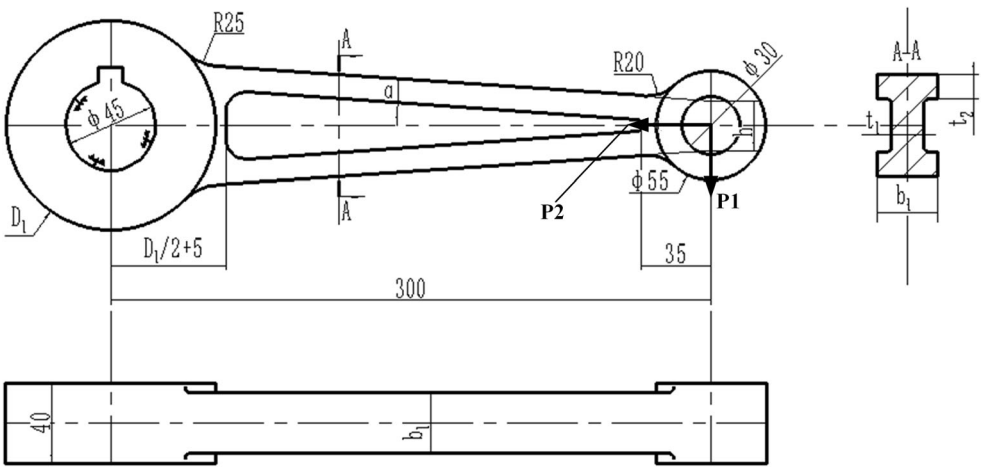

Fig. 13 Geometry and parameterization of the torque arm

Table 11 The value of the forces and the material parameters for the torque arm

P1	8.0 kN
P2	4.0 kN
Young's modulus	200 GPa
Poisson's ratio	0.3

reference cases. Quality metrics of NSGA-II with HF models are listed in Table 8. The box charts of the RHD, OS, and FC obtained under different value of $r\%$ are shown in Fig. 7. On each box, the central mark is the median, the edges of the box are the 25th and 75th percentiles, the whiskers extend to the most extreme data points not considered outliers, and outliers are plotted individually.

It can be seen in Table 7, Table 8, and Fig. 7, the value of r has little effect on the efficiency of the approach in terms of the computational efficiency for all the cases. For ZDT1 example and ZDT2 example, the mean values of RHD and OS are closest to that of NSGA-II with HF models while $r\% = 80\%$ that indicates that the proposed approach shows the best performance for the convergence and diversity of Pareto optimum. Meanwhile, the smallest value of STD means the best stability while $r\% = 80\%$. For the FON example, the RHD and OS of the proposed approach are closest to that of NSGA-II with HF models and show the best stability while $r\% = 80\%$. For the POL example, the average value of RHD and OS is not obvious to the change of value of r, but the proposed approach shows better stability while $70\% \le r\% \le 90\%$.

Considering the comparison results of the four examples, we finally set r as 80 in this paper.

4.2.2 Comparison with other approaches

We solved four numerical problems 30 times for different approaches to account for the influence of randomness. As demonstration, we use a numerical example (ZDT2) to present a detailed comparison of different approaches first.

Figure 8 demonstrates a typical set of Pareto frontiers obtained from one of the 30 runs of different approaches. As shown in Fig. 8, the Pareto frontiers obtained by four metamodel-based approaches are in good agreement with that obtained by NSGA-II with HF model, while only a small portion of the Pareto frontiers from NSGA-II with LF model and NSGA-II with HF model overlaps. It can be concluded that incorporating LF models directly into the MOGA may obtain inaccurate Pareto frontiers.

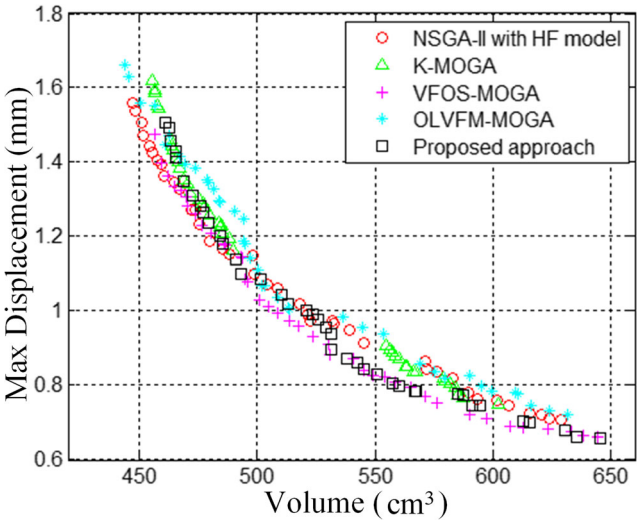

Fig. 15 The typical Pareto frontiers obtained by different approaches for the design of the torque arm

The comparison results of different approaches are summarized in Table 9. The box charts of the RHD, OS, and FC obtained by different approaches for ZDT problem are shown in Fig. 9. From Table 9 and Fig. 9, it can be seen that the range, mean value, and STD of RHD and OS obtained by the proposed approach are closest to that obtained by NSGA-II with the HF model. That means, the proposed approach can solve the multi-objective problem precisely. Meanwhile, the proposed approach shows very good stability.

In terms of the computational efficiency, the FC of the proposed approach is far less than that of NSGA-II with HF model and VFOS-MOGA. Meanwhile, the average FC of the proposed approach is reduced by 39% compared to K-MOGA and 22% compared to OLVFM-MOGA. The reasons are as follows: (1) All the individuals will be evaluated by the HF model in NSGA-II with HF model; (2) In VFOS-MOGA, evaluating the fitness value of all individuals needs to call LF models and the computational cost of LF model cannot be ignored; (3) The K-MOGA is based on the Kriging model

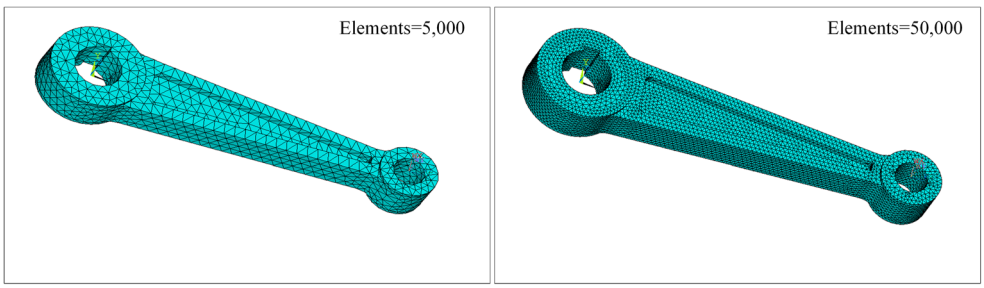

(a) LF simulation model (b) HF simulation model

Fig. 14 HF/LF simulation model of the torque arm

Table 12 Comparison results of different approaches for the design of the torque arm

	NSGA-II with HF models	K-MOGA			VFOS-MOGA			OLVFM-MOGA			Proposed approach		
		15 runs	Mean	STD	15 runs	Mean	STD	15 runs	Mean	STD	15 runs	Mean	STD
RHD	0.37	(0.29 0.40)	0.35	0.03	(0.28 0.30)	0.29	0.004	(0.32 0.42)	0.36	0.02	(0.28 0.34)	0.30	0.02
OS	0.22	(0.15 0.33)	0.24	0.07	(0.14 0.21)	0.17	0.015	(0.20 0.39)	0.26	0.05	(0.16 0.26)	0.20	0.03
FC	3840	(127 429)	174.73	91.37	(1386 1395)	1391	3.137	(100 216.25)	143.22	32.01	(78.00 103.75)	89.68	6.39

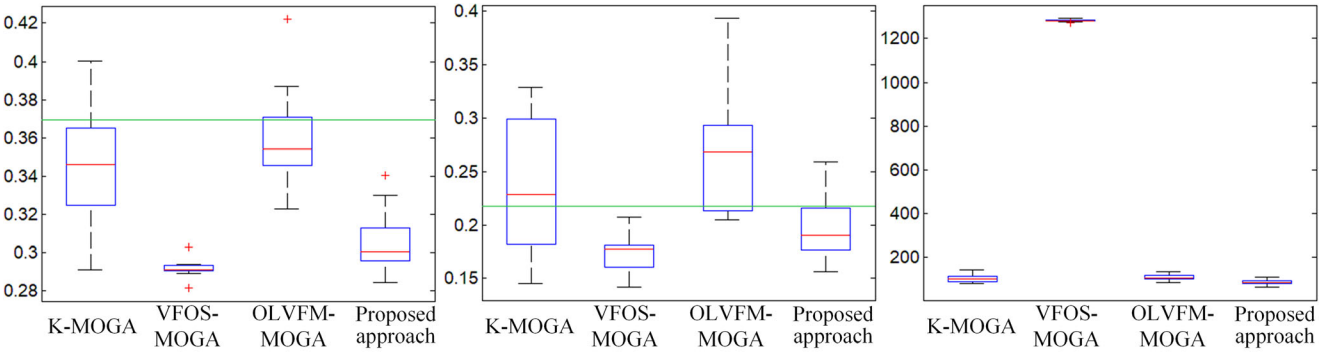

(a) Box chart of RHD (b) Box chart of OS (c) Box chart of FC

Fig. 16 The box charts of different approaches for the design of the torque arm

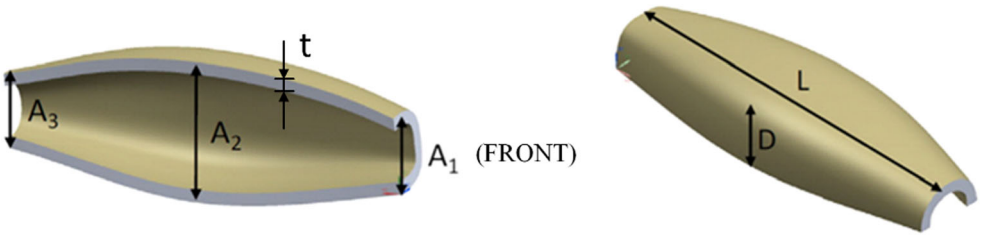

Fig. 17 The geometry of MAV fuselage with general dimension labels

constructed by HF sample points and the HF model is much more time consuming than the LF model; (4) The proposed approach can make full use of the information from the LF model and reduce the metamodel uncertainty by adding cheap LF sample points; (5) The proposed approach can prevent the cluster of sample points. To demonstrate the fourth reason, the number of HF/LF sample points in the 30 runs of the proposed approach are plotted in Fig. 10. It can be seen that the proposed approach utilizes a lot of LF sample points to improve the accuracy of a metamodel. Because of the cheap computational cost of LF sample points, this can really help to improve the efficiency of MOGA.

Table 13 The ranges of the design variables of MAV fuselage

Design variables	Lower bound (mm)	Upper bound (mm)
A_1	46.0	50.0
A_2	85.0	95.0
A_3	40.0	46.0
D	40.0	50.0
L	250.0	260.0
t	6	8

The obtained Pareto frontiers of the remaining three numerical examples using different approaches are shown in Fig. 11. The comparison results for the quality of Pareto solutions and computational efforts are summarized in Table 10. The box charts of the RHD, OS, and FC obtained by different approaches for the three problems are shown in Fig. 12. It can be concluded that K-MOGA, VFOS-MOGA, OLVFM-MOGA, and the proposed approach can obtain satisfactory optimal solutions. In terms of efficiency, the proposed approach needs least computational cost. Compared to K-MOGA, VFOS-MOGA, and OLVFM-MOGA, the computational cost of the proposed approach is reduced by 76%, 94%, and 70% respectively for ZDT1 problem, and 76%, 95%, and 67% for FON problem. For POL problem, the FC average is reduced to 17%, 93%, and 21% compared to K-MOGA, VFOS-MOGA, and OLVFM-MOGA.

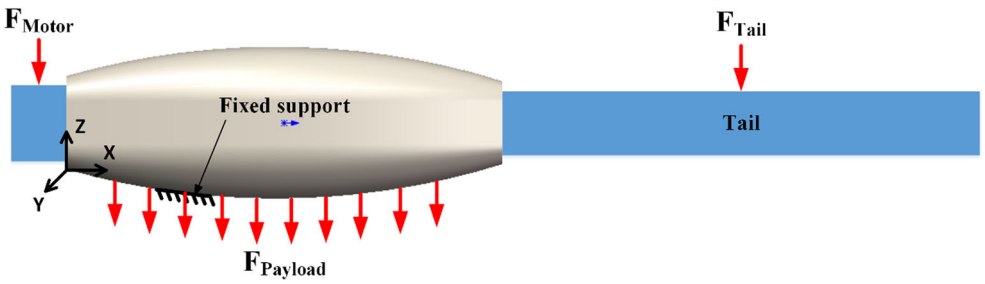

Fig. 18 Loading and boundary conditions for the MAV fuselage

4.3 Design optimization of a torque arm

In this section, the proposed approach is applied to the design optimization of a torque arm. As shown in Fig. 13, the torque arm is fixed to the hole at the left end. P1 and P2 are placed at the center of the right end. The value of the forces and the material parameters are listed in Table 11.

There are six design variables for the design of the torque arm: α, b_1, D_1, h, t_1, and t_2. The design optimization of the torque arm can be expressed as follows,

$$\begin{aligned} &\min f_1 = V(\alpha, b_1, D_1, h, t_1, t_2) \\ &\min f_2 = \max\_d(\alpha, b_1, D_1, h, t_1, t_2) \\ &s.t. \quad g_1 = \sigma \le 190MPa \\ &\text{where } 3\ \text{deg} \le \alpha \le 4.5\text{deg}; 25\text{mm} \le b_1 \le 35\text{mm}; \\ &\quad 90\text{mm} \le D_1 \le 120\text{mm}; 20\text{mm} \le h \le 30\text{mm}; \\ &\quad 12\text{mm} \le t_1 \le 22\text{mm}; 8\text{mm} \le t_2 \le 12\text{mm} \end{aligned} \tag{11}$$

where V is the total volume of the torque arm, max _ d is the maximum displacement. In the optimization process, the maximum displacement and stress of the torque arm are calculated by the VF metamodel. LF simulation model contains 5 thousand elements while HF simulation model contains 50 thousand elements as shown in Fig. 14. ANSYS Parametric Design Language (APDL) is used for modeling and simulation. The computational cost of the HF model is four times the cost of the LF model ($T = 4$).

The three metamodel-based approaches are calculated 15 times due to the randomness of MOGA. Since the computational cost of MOGA with HF model is very high, it is only run one time. The typical Pareto frontiers obtained by different approaches are plotted in Fig. 15.

As shown in Fig. 15, the Pareto frontiers obtained by different approaches are in good consistency. The comparison results are summarized in Table 12. The box charts of different approaches for the design of the torque arm are shown in Fig. 16. In Fig. 16 a and b, the two green lines represent the value of RHD and OS obtained by NSGA-II with HF models.

As illustrated in Table 12, the four metamodel-based approaches can obtain satisfying Pareto frontiers according to the values of RHD and OS. It can be seen in Fig. 16 that the proposed approach is superior to K-MOGA and OLVFM-MOGA in the stability of RHD and OS. In terms of the computational cost, the FC of the proposed approach is far less than that of NSGA-II with HF model and VFOS-MOGA. Compared to K-MOGA and OLVFM-MOGA, the average FC of the proposed approach is reduced by 48% and 37%, respectively.

4.4 Design of micro-aerial vehicle fuselage

The proposed approach is applied to the design of micro-aerial vehicle (MAV) fuselage. In this design example, the fuselage

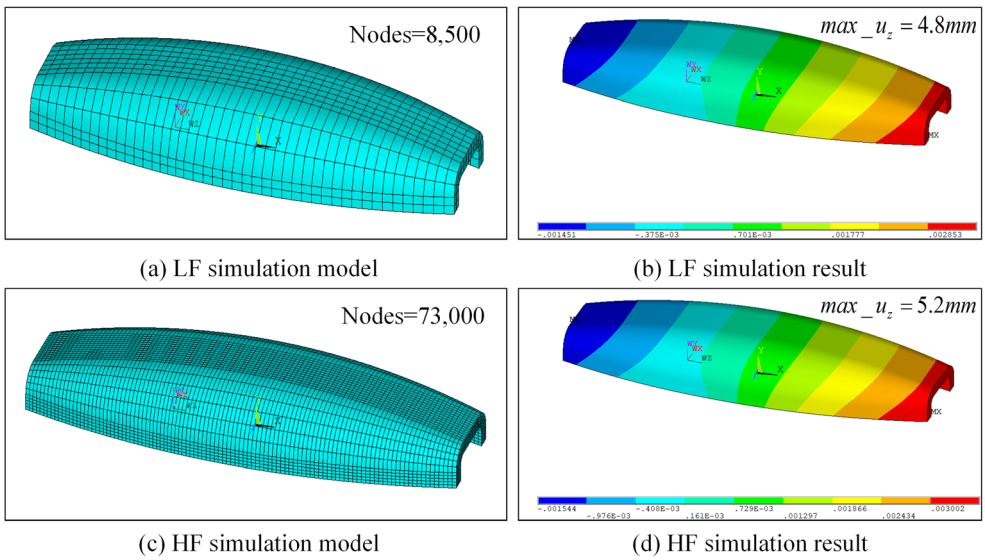

(a) LF simulation model (b) LF simulation result

(c) HF simulation model (d) HF simulation result

Fig. 19 The HF/LF simulation models and simulation results for MAE

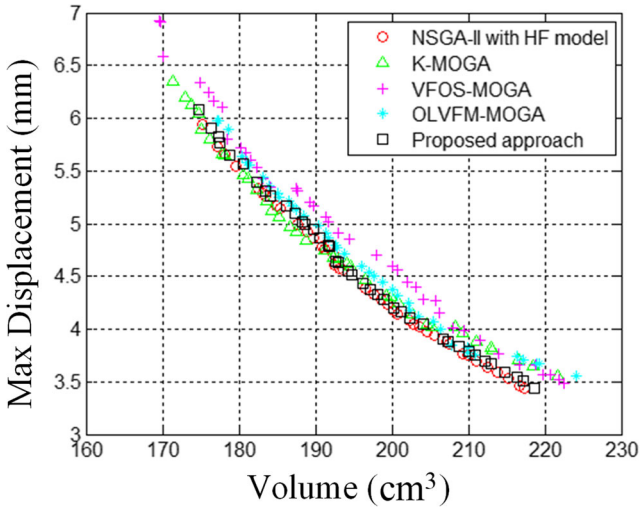

Fig. 20 The obtained Pareto frontiers using different approaches for the design of MAE fuselage

is made of lightweight ABS material. Young's modulus is 1960 N/mm^2 and Poisson's ratio is 0.3. The geometric model of the MAV fuselage is shown in Fig. 17. Table 13 gives the ranges of design variables.

As shown in Fig. 18, the weight of the engine in the front $F_{\text{Motor}} = 5.9N$and the weight of the tail $F_{\text{Tail}} = 2.7N$ are simplified as concentrated loads acting at their centers of gravity which are applied in ANSYS with weightless rigid link elements. The payload $F_{\text{Payload}} = 0.\ 1\text{N/mm}^2$ serves as a distributed load on the internal surface of MAV fuselage. The weight of the wing can be negligible. A small area at the bottom of the fuselage is fixed to model the contact area when landing or crashing.

The design optimization of the MAV fuselage can be expressed as follows,

$$\begin{aligned} &\min f_1 = V(A_1, A_2, A_3, D, L,\ t) \\ &\min f_2 = \max\_u_z(A_1, A_2, A_3, D, L,\ t) \\ &s.t.\ \ g_1 = \sigma \leq 40MPa \end{aligned} \tag{12}$$

where V is the total volume of the MAV fuselage, max _ u_z is the maximum displacement along the z-axis. The simulation model with about 8.5 thousand nodes is chosen as the LF model while the simulation model with about 73 thousand nodes is chosen as the HF model. The HF/LF simulation models and simulation results of MAE in the same set of parameters are shown in Fig. 19. The modeling and simulation time of obtaining a HF sample is about 6 times that of obtaining a LF sample ($T = 6$).

K-MOGA, OLVFM-MOGA, and the proposed approach are calculated 15 times while NSGA-II with HF models and VFOS-MOGA are only calculated one time because of their high computational cost. Figure 20 plotted the typical Pareto frontiers obtained from different approaches.

As shown in Fig. 20, most of the Pareto frontiers obtained by four metamodel-based approaches and NSGA-II with HF

Table 14 Comparison results of different approaches for the design optimization of MAE

	NSGA-II with HF model	VFOS-MOGA	K-MOGA			OLVFM-MOGA			Proposed approach		
			15 runs	Mean	STD	15 runs	Mean	STD	15 runs	Mean	STD
RHD	0.35	0.44	(0.35 0.44)	0.40	0.03	(0.37 0.49)	0.42	0.03	(0.37 0.45)	0.39	0.03
OS	0.41	0.71	(0.36 0.66)	0.52	0.09	(0.43 0.89)	0.63	0.12	(0.39 0.52)	0.45	0.03
FC	3849	1388	(100 132)	114.20	9.40	(85.5 147)	111.30	15.47	(104.83 141.83)	102.28	8.10

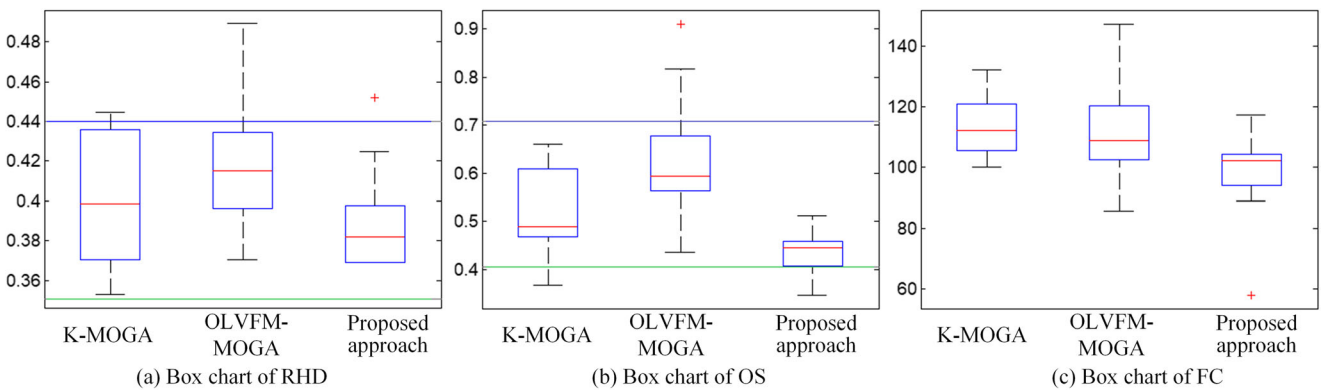

Fig. 21 The box charts of different approaches for the design of the torque arm

model overlap. That means, all of these methods can obtain approximate Pareto optimal solutions. The Pareto solutions obtained by the proposed approach agree best with the Pareto solutions obtained by NSGA-II with HF models. To further compare the quality and efficiency of different approaches, the RHD, OS, and FC are calculated and summarized in Table 14. The box charts of different approaches for the design of the MAE fuselage are shown in Fig. 21. In Fig. 21 a and b, the two green lines represent the value of RHD and OS obtained by NSGA-II with HF models, and the two blue lines represent the value of RHD and OS obtained by VFOS-MOGA.

As shown in Table 14 and Fig. 21, the computational cost of VFOS-MOGA is still very expensive while the computational cost of LF simulation models cannot be ignored. The FC of the proposed approach is far less than that of NSGA-II with HF model and VFOS-MOGA. Meanwhile, the average FC of the proposed approach is reduced by about 11% compared to K-MOGA and 8% compared to OLVFM-MOGA.

5 Conclusion

In this work, a novel VF optimization approach for multi-objective design optimization is proposed, in which a VF metamodel is embedded in the original NSGA-II to replace expensive simulation models. The optimization process is divided into exploration stage and exploitation stage. For each stage, an algorithm is proposed to select candidate HF/LF sample points considering the VF metamodel uncertainty and computational cost of HF/LF models. To avoid the clustering of sample points, a criterion is developed to select HF/LF sample points from candidates.

The proposed approach is applied to four numerical problems and two engineering problems. To demonstrate the applicability and efficiency of the proposed approach, the proposed approach is compared with four other approaches. The results show that the proposed approach can obtain satisfactory Pareto frontier with good quality for all the problems. In terms of computational cost, it can be concluded that the proposed approach is more efficient than other four approaches.

In the future work, developing the proposed approach to high dimension problems will be investigated.

Acknowledgments The authors also would like to thank the anonymous referees for their valuable comments.

Funding information This research has been supported by the National Natural Science Foundation of China (NSFC) under Grant No. 51775203, No. 51805179, No. 51721092, and the Fundamental Research Funds for the Central Universities, HUST: Grant No. 2016YXMS272.

Compliance with ethical standards

Conflict of interest The authors declare that they have no conflict of interest.

References

Ak R, Li Y, Vitelli V, Zio E, López Droguett E, Magno Couto Jacinto C (2013) NSGA-II-trained neural network approach to the estimation of prediction intervals of scale deposition rate in oil & gas equipment. Expert Syst Appl 40:1205–1212

An H, Chen S, Huang H (2018) Multi-objective optimization of a composite stiffened panel for hybrid design of stiffener layout and laminate stacking sequence. Struct Multidiscip Optim 57:1411–1426

Andrés E, Salcedo-Sanz S, Monge F, Pérez-Bellido AM (2012) Efficient aerodynamic design through evolutionary programming and support vector regression algorithms. Expert Syst Appl 39:10700–10708

Chen G, Han X, Liu G, Jiang C, Zhao Z (2012) An efficient multi-objective optimization method for black-box functions using sequential approximate technique. Appl Soft Comput 12:14–27

Cheng R, Jin Y, Narukawa K, Sendhoff B (2015a) A multiobjective evolutionary algorithm using Gaussian process-based inverse modeling. Evolutionary Computation, IEEE Transactions on 19: 838–856

Cheng S, Zhou J, Li M (2015b) A new hybrid algorithm for multi-objective robust optimization with interval uncertainty. J Mech Des 137:021401

Datta R, Regis RG (2016) A surrogate-assisted evolution strategy for constrained multi-objective optimization. Expert Syst Appl 57: 270–284

Deb K, Pratap A, Agarwal S, Meyarivan T (2002) A fast and elitist multiobjective genetic algorithm: NSGA-II. Evolutionary Computation, IEEE Transactions on 6:182–197

Gano SE, Renaud JE, Martin JD, Simpson TW (2006) Update strategies for kriging models used in variable fidelity optimization. Struct Multidiscip Optim 32:287–298

Goel T, Vaidyanathan R, Haftka RT, Shyy W, Queipo NV, Tucker K (2007) Response surface approximation of Pareto optimal front in multi-objective optimization. Comput Methods Appl Mech Eng 196:879–893

Hamdaoui M, Oujebbour F-Z, Habbal A, Breitkopf P, Villon P (2015) Kriging surrogates for evolutionary multi-objective optimization of CPU intensive sheet metal forming applications. Int J Mater Form 8: 469–480

Han Z-H, Zimmermann R, Goretz S (2010) A new cokriging method for variable-Fidelity surrogate modeling of aerodynamic data. In: 48th AIAA aerospace sciences meeting including the new horizons forum and aerospace exposition. p 1225

Huang D, Allen TT, Notz WI, Miller RA (2006) Sequential kriging optimization using multiple-fidelity evaluations. Struct Multidiscip Optim 32:369–382

Koch P, Yang R-J, Gu L (2004) Design for six sigma through robust optimization. Struct Multidiscip Optim 26:235–248

Li M (2011) An improved kriging-assisted multi-objective genetic algorithm. J Mech Des 133:071008-071008-071011

Li G, Li M, Azarm S, Rambo J, Joshi Y (2007) Optimizing thermal design of data center cabinets with a new multi-objective genetic algorithm. Distributed and Parallel Databases 21:167–192

Li M, Li G, Azarm S (2008) A kriging metamodel assisted multi-objective genetic algorithm for design optimization. J Mech Des 130:031401

Li G, Li M, Azarm S, Al Hashimi S, Al Ameri T, Al Qasas N (2009) Improving multi-objective genetic algorithms with adaptive design

of experiments and online metamodeling. Struct Multidiscip Optim 37:447–461

Liu Y, Collette M (2014) Improving surrogate-assisted variable fidelity multi-objective optimization using a clustering algorithm. Appl Soft Comput 24:482–493

Luo J, Gupta A, Ong Y-S, Wang Z (2018) Evolutionary optimization of expensive multiobjective problems with co-sub-Pareto front Gaussian process surrogates. IEEE Transactions on Cybernetics

McKay MD, Beckman RJ, Conover WJ (2000) A comparison of three methods for selecting values of input variables in the analysis of output from a computer code. Technometrics 42:55–61

Nguyen J, Park SI, Rosen D (2013) Heuristic optimization method for cellular structure design of light weight components. Int J Precis Eng Manuf 14:1071–1078

Ollar J, Mortished C, Jones R, Sienz J, Toropov V (2017) Gradient based hyper-parameter optimisation for well conditioned kriging metamodels. Struct Multidiscip Optim 55:2029–2044

Park H-S, Dang X-P (2010) Structural optimization based on CAD–CAE integration and metamodeling techniques. Comput Aided Des 42: 889–902

Rahmani S, Ebrahimi M, Honaramooz AA (2018) Surrogate-based optimization using polynomial response surface in collaboration with population-based evolutionary algorithm. In: Schumacher A, Vietor T, Fiebig S, Bletzinger K-U, Maute K (eds) Advances in Structural and Multidisciplinary Optimization. Springer International Publishing, Cham, pp 269–280

Regis RG (2014) Evolutionary programming for high-dimensional constrained expensive black-box optimization using radial basis functions. Evolutionary Computation, IEEE Transactions on 18: 326–347

Shan S, Wang GG (2005) An efficient Pareto set identification approach for multiobjective optimization on black-box functions. J Mech Des 127:866–874

Shi Y, Reitz RD (2010) Assessment of multiobjective genetic algorithms with different niching strategies and regression methods for engine optimization and design. J Eng Gas Turbines Power 132:052801

Shu L, Jiang P, Wan L, Zhou Q, Shao X, Zhang Y (2017) Metamodel-based design optimization employing a novel sequential sampling strategy. Eng Comput 34:2547–2564

Shu L, Jiang P, Zhou Q, Shao X, Hu J, Meng X (2018) An on-line variable fidelity metamodel assisted multi-objective genetic algorithm for engineering design optimization. Appl Soft Comput 66: 438–448

Song Z, Murray BT, Sammakia B, Lu S (2012) Multi-objective optimization of temperature distributions using artificial neural networks. In: Thermal and Thermomechanical Phenomena in Electronic Systems (ITherm), 2012 13th IEEE intersociety conference on. IEEE, pp 1209–1218

Sun X, Gong D, Jin Y, Chen S (2013) A new surrogate-assisted interactive genetic algorithm with weighted semisupervised learning. Cybernetics, IEEE Transactions on 43:685–698

Sun C, Jin Y, Cheng R, Ding J, Zeng J (2017) Surrogate-assisted cooperative swarm optimization of high-dimensional expensive problems. IEEE Trans Evol Comput 21:644–660

Wang H, Jin Y, Jansen JO (2016) Data-driven surrogate-assisted multiobjective evolutionary optimization of a trauma system. IEEE Trans Evol Comput 20:939–952

Wu J, Azarm S (2001) Metrics for quality assessment of a multiobjective design optimization solution set. J Mech Des 123:18–25

Zhou Q, Shao X, Jiang P, Cao L, Zhou H, Shu L (2015) Differing mapping using ensemble of metamodels for global variable-fidelity metamodeling. Comput Model Eng Sci 106:323–355

Zhou Q, Wang Y, Choi S-K, Jiang P, Shao X, Hu J (2017) A sequential multi-fidelity metamodeling approach for data regression. Knowl-Based Syst 134:199–212

Zhu J, Wang Y-J, Collette M (2013) A multi-objective variable-fidelity optimization method for genetic algorithms. Eng Optim 46:521–542